Eur. Phys. J. D **16**, 219–223 (2001)

THE EUROPEAN PHYSICAL JOURNAL D

EDP Sciences

Optical and electrical properties of hydrogenated yttrium nanoparticles

G. Bour[a], A. Reinholdt, A. Stepanov, C. Keutgen, and U. Kreibig

I. Physikalisches Institut 1A der RWTH Aachen, D-52056 Aachen, Germany

Received 29 November 2000

Abstract. We studied the effect of hydrogen in yttrium nanoparticles on a quartz substrate, using optical spectroscopy and electrical resistance measurements. Pulsed laser deposition is used to obtain the Y clusters in an UHV environment. We show, that these clusters are highly sensitive to monoatomic H_1 produced from ambient hydrogen gas pressures, ranging from 10^{-5} to 50 mbar with our experimental arrangement. The changes of optical and electrical properties due to the chemical reaction within the particles are sufficient to consider this material as a possible sensor for low concentrations of hydrogen.

PACS. 71.30.+h Metal-insulator transitions and other electronic transitions – 73.63.Bd Nanocrystalline materials – 78.66.-w Optical properties of specific thin films

1 Introduction

With novel cluster production and characterization techniques we have been successful in producing metallic yttrium clusters using PLD (pulsed laser deposition). Yttrium close to the group of rare earth elements had not yet had the attention of traditional cluster science. Its application in television tubes and in laser systems, in combination with other materials, show its potentially interesting optical behaviour. However, preparation of yttrium nanoparticles is extremely difficult as its affinity to oxygen, $\Delta H_f = -1906.6$ kJ mol^{-1} [1], only allows this material to be suitably processed and investigated in UHV.
Bulk yttrium has remarkable features. Under the presence of atomic hydrogen one can observe electronic and structural phase changes, following reaction sequence 1, see [2]

$$\mathrm{Y} + 3\mathrm{H}_1 \overset{\Delta H_f = -114\ \mathrm{kJ\,mol^{-1}}\ [3]}{\rightharpoonup} \mathrm{YH}_2 + \mathrm{H}_1 \overset{\Delta H_f = -41.8\ \mathrm{kJ\,mol^{-1}}\ [4]}{\rightleftharpoons} \mathrm{YH}_{3-\delta},\ \delta < 1. \quad (1)$$

The dihidride-trihidride phase transitions are reversible at room temperature, which makes this material a potential hydrogen sensor, capable of detecting slight increases in H_2 pressure. For the first time we have been able to show the electronic phase transition in nanoparticles simultaneously by electrical and optical means.

2 Sample preparation

The nanoparticle system under consideration in this paper has been prepared by PLD. A Nd:YAG laser (*Lumonics JK702 H*) delivered 300 mJ per pulse with a wavelength of 1064 nm. The pulse duration was 1 ms, the pulse frequency 80 Hz. The energy density at the surface of the target was kept constant at 4.7 J cm^{-2} per pulse.

An Yttrium target, $\emptyset$ 12.7 mm (*Alfa*), was loaded into the ablation chamber after removing any residual yttrium-oxide films. To achieve a supersonic cluster jet, [5–8], a constant flow (either 2.5 l min^{-1} or 7.5 l min^{-1}) of purified argon gas (Ar 6.0, *Air Products*) is directed into the ablation chamber yielding a pressure inside this chamber of about 4 bar. Using a differential pumping system, the Ar pressure in the measurement chamber can be kept at 7×10^{-5} mbar during ablation, the base pressure is below 1.0×10^{-8} mbar. The experimental equipment is shown in Fig. 1.

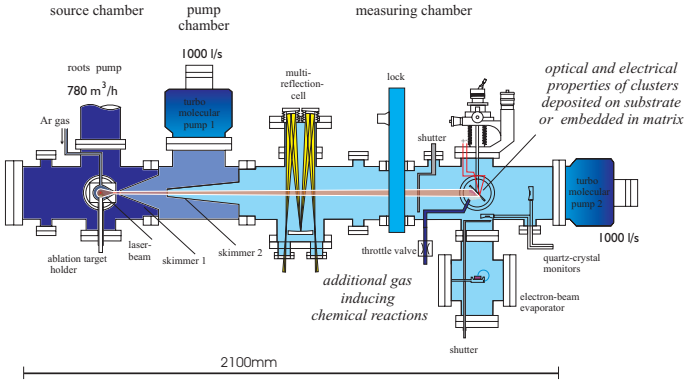

Fig. 1. Experimental set-up. Three differential pumping stages, together with Ar seeding gas, allow supersonic expansion of the cluster beam from the source chamber into the measurement chamber.

[a] e-mail: giorah.bour@physik.rwth-aachen.de

The nanoparticles can either be deposited onto a quartz substrate (25 × 75 mm, *Heraeus Suprasil*) or a quartz crystal oscillator (*Leybold XTC*) to control the mass deposition per pulse. First however, the laser is used to evaporate the top most layer of the target, to further eliminate oxygen from the target surface.

For the electrical conductivity four contacts were used in a square geometry, 4.5 mm apart. They were deposited on the quartz substrate either using DC magnetron sputtering or PVD. First an adhesive layer of 40 nm titanium was deposited, after which a 100 nm gold film made the actual contacts. Wired, gold coated pogo sticks (*Everett Charles Technologies*) were put on top of these contacts, without scratching the gold surface. This set-up allows simultaneous *in situ* optical and electrical measurements. A source measure unit (*Keithley 236*) is used to evaluate the current signal, which is usually between fA and nA at 1 V.

For the optical experiment we used a XBO lamp, which is focussed on a 2 mm spot between the electrical contacts on the sample. Using fiber optics, the transmitted light is then evaluated with a multichannel spectrometer (*Zeiss MCS 400*) in the range is 1.3 eV to 6 eV.

The ablation process, the nucleation and the particle growth, in general very complicated, are dynamic processes, far away from equilibrium. A lot of work is still needed to fully understand them. Our results indicate, that the mean particle size depends on the actual Ar flow and the ambient pressure used during ablation. A similar behaviour has been reported for different materials [9–11]. For yttrium we find from TEM micrographs (*we are indebted for these investigations to the GfE RWTH Aachen)*, that with higher ambient Ar pressures mean particle sizes and their standard deviations are increased, see Fig. 2. Some particles show distinguishable signs of coagulation and coalescence. Furthermore, almost all yttrium particles under investigation have a very thin shell, presumably oxygen, see Fig. 3. The non-coagulated particles seem to

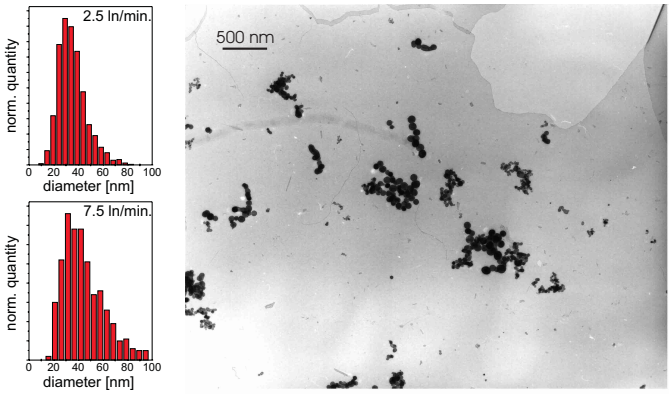

Fig. 2. Size distributions for different Ar flows (2.5 $\mathrm{l\,min^{-1}}$, (a), and 7.5 $\mathrm{l\,min^{-1}}$, (b)). Larger mean diameters (38.8 nm compared to 32.5 nm) and broader size distributions are found at higher Ar flows. The TEM micrograph taken for submonolayer coverage, belongs to the lower size distribution, (b).

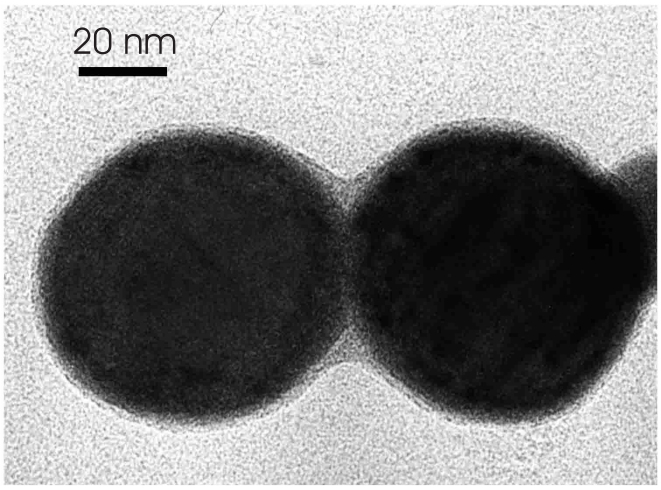

Fig. 3. HRTEM micrograph of yttrium nanoparticles. Clearly distinguishable is the shell, presumably consisting of yttriumoxide, which prevents further particle regrowth.

be separated by this shell. This would indicate oxidation during ablation, *i.e.* before particle regrowth, which would inhibit particle regrowth. This means, although we have percolated films, needed for electrical measurements, we can still assume separated nanoparticles to be present and apply Mie's theory [13] as an acceptable approximation. For the hydrogenation process these shells do not matter significantly.

As hydrogen can only be absorbed in its monoatomic form and not as H_2, we used a thin (thickness 5 nm) Pd film as a catalyst, see for example [14]. This film was deposited on top of the gold contacts and the quartz substrate and then cut with a razor blade to exclude any conductivity. In our experiments we did not detect any noticeable change of the optical transmittance and the electrical conductivity of the Pd film during hydrogenation. The yttrium particles were deposited on top of the non-conducting Pd film, after which molecular hydrogen gas was let into the measurement chamber.

3 Experimental results

Both bulk yttrium and $YH_{\approx 2}$ have metallic character whereas $YH_{3-\delta}, \delta < 1$ shows dielectric behavior. We use this feature, which we previously found also to exist in nanoparticles, [18], to distinguish between these two electronic phases. Comparison of experimental optical data with basic Mie theory can be used to discriminate between the two metallic phases, which exhibit different Mie peaks and the dielectric phase, which does not show any plasmon peak.

Electrical resistivity data are capable of distinguishing between both hydride phases. Both methods are proficient in observing and describing the metal-insulator transition in detail. In fact, they complement each other, as the optical properties are especially sensitive for investigating the beginning of the transition at low hydrogen amounts,

whereas the electrical changes can be exploited at medium and high hydrogen amounts.

3.1 Optical experiments

Optical properties are by nature very sensitive to any change in the electronic structure. This holds even more for nanoparticles, where sharp and distinct Mie peaks can appear. Both yttrium and its metallic hydride phase possess resonance maxima in our measurement range of 1 eV to 5 eV.

In the measurement range investigated by us, $YH_{\approx 2}$ has two Mie resonances, one at 1.26 eV and one at 3.25 eV. Going from yttrium to yttrium dihydride, we first observe the peak at 3.25 eV and then at 1.26 eV, see (a) in Fig. 4.

The best fit with theoretical Mie calculations, see (b) in Fig. 4, can be made assuming $YH_{2.2}$. This assures a quantitatively correct ratio between the peak at 1.3 eV and 3.3 eV. For these calculations bulk dielectric functions were used, obtained from [15–17]. A difference between theory and experiment is, that both experimental peak positions differ slightly from the calculated ones. This is however within the experimental margin of error, as these calculated peaks shift with the hydrogen amount inside the nanoparticles, which is unknown in our experiment and can only be determined from these optical features. Additionally, we do not see the slight shoulder at 2.2 eV in the calculations, see (b) in Fig. 4.

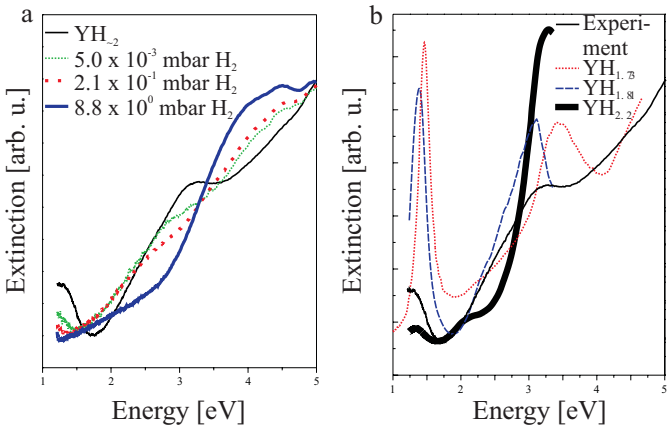

Fig. 4. Experimental (a) and calculated (b) spectra at different hydrogen pressures. Size distributions are not included in the calculations, instead mean particle sizes of 32 nm were assumed.

As more and more hydrogen is being built into the $YH_{\approx 2}$ lattice, two noticeable changes can be seen from (a) in Fig. 4. The peak at 1.26 eV disappears rapidly and has vanished at 2.1×10^{-1} mbar external H_2 pressure. The peak at 3.25 eV remains visible longer (as a shoulder), but at 8.8 mbar has faded away as well. This process and therefore the spectra are reversible, as predicted by Eq. (1), thus rendering the dihidride → trihidride transition most interesting.

The dielectric phase can be treated as a large band gap semiconductor. Extracting the slope of the interband edge at 8.8 mbar H_2 in Fig. 4(a), we estimate the band gap to be about 2.51 eV. This is in agreement with our previous optical results [18] at similar hydrogen pressures, which proves the general features of hydrogenation of yttrium nanoparticles even for strongly differing sample topologies. Probably hydrogen pressure could be increased even more and yield a continuing change, as the slope still has the remains of the peak at 3.25 eV in its tail in Fig. 4(a). This implies the metal-insulator transition is not complete.

In summary we are able to clearly distinguish optically between the range of 5×10^{-3} mbar to 8.8 mbar hydrogen pressure, using the reversible hydrogenation of yttrium dihidride to trihydride and the accompanying electronic phase change noted in Eq. (1).

3.2 Electrical investigations

The conduction mechanism in a percolated film is very complicated in general. As we will exploit the reversibility of our system, theoretical calculations to model the system will be avoided for now. The focus is on the possibility of this system to change its electronic state in such a way, that the conduction regime is changed as well. Any reversible change in resistivity will be ascribed to the electronic phase transition.

It is difficult to distinguish yttrium from yttrium dihidride by electrical means, as both phases are metallic in nature. The presence of Mie resonances presented above proved this metallic behavior once more. However, it should be possible to distinguish between $YH_{\approx 2}$ and $YH_{3-\delta}$. Optical measurements are used as reference, as changes in the optical spectra can directly be linked to the metal-insulator transition, as shown above.

In Fig. 5(a) the change in resistivity over time with respect to H_2 is presented. We started out at 3×10^{-6} mbar background pressure, which still remained after deposition. Increasing the pressure to 2×10^{-5} mbar H_2 resulted in a minor change of 16 Ω in resistivity of the sample over 30 minutes. This amounts to 0.1% of the total resistivity present. From the first inset (I) in Fig. 5(a) it can be seen, that the sample is almost in equilibrium with the hydrogen pressure and the resistivity does not increase any further.

The second increase in H_2 partial pressure to 1×10^{-5} mbar resulted in a more pronounced change of 146 Ω over 47 minutes, yielding a change of 1%. The second inset (II) in Fig. 5(a) does not yet show signs of having reached equilibrium, as the curve still increases further.

Every increase in hydrogen pressure afterwards has pronounced effects on the resistivity. At 1×10^{-3} mbar and 1×10^{-2} mbar respectively, equilibrium is reached within 30 minutes. For higher pressures this is not the case any more. At these pressures a rapid change within minutes is observed, followed by a gradual increase, which does not reach equilibrium within the time of experiment, giving rise to the assumption more than one diffusion mechanism is present.

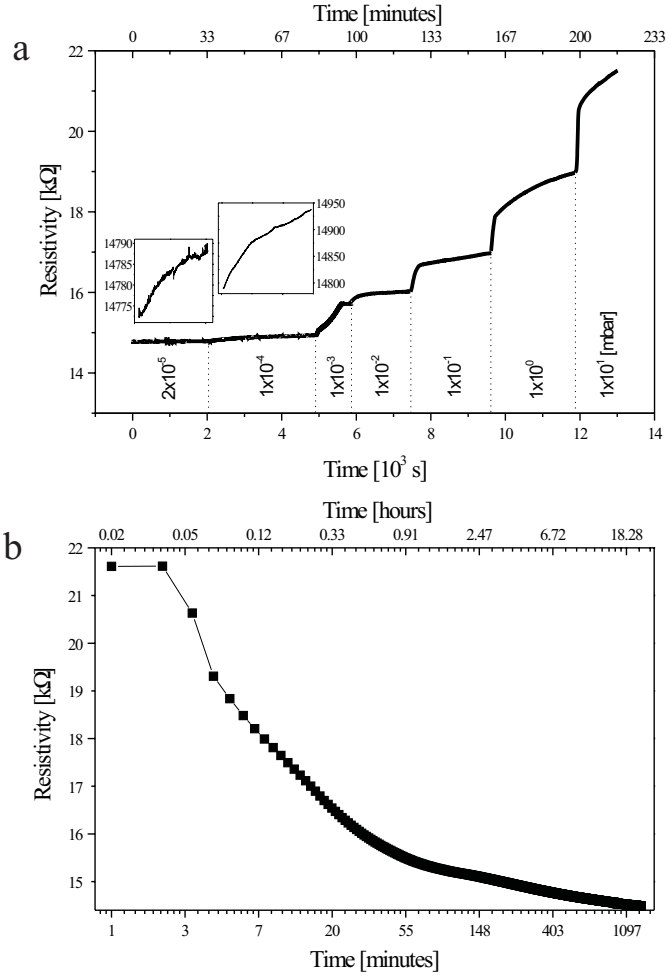

Fig. 5. Change in resistivity of the yttrium nanoparticle sample with respect to to hydrogen supply over time. Dependency of increase of hydrogen pressure is presented in (a). Inset I and II show a more detailed view. The dependency of decrease of hydrogen pressure to 1.5×10^{-6} mbar is presented in (b). Measurements were made every second.

A similar time dependency can be observed during the decrease in hydrogen pressure by pumping off the H_2, see Fig. 5(b). The reaction speed is obviously slower than before, which can be deduced in Eq. (1) from the heat of formation. First we see a rapid decrease in resistivity, which takes less than an hour. After 30 minutes the pressure was below 1×10^{-5} mbar. However 21 hours were needed to return to the resistivity, that was measured before the initial increase in hydrogen. And still no equilibrium has been reached as obvious from the slope of the curve. Possibly the Pd film is responsible for this behavior, as Pd is known to absorb hydrogen. Hydrogen desorbing from Pd can, in our system, be absorbed once more by yttrium, therefore reducing reaction speed. It should be noted, that no noticeable change in resistivity was detected of the pure Pd film at the pressures in this experiment.

The measurements in Fig. 4 and in Fig. 5 were performed simultaneously. Our experiments show, that optical measurements are sensitive especially in the range between 1×10^{-3} mbar and 1×10^{-1} mbar. Electrical measurements are highly sensitive above 1×10^{-2} mbar, however also show changes at very low pressures.

4 Summary

We have shown it is possible to create yttrium nanoparticles with different sizes using laser ablation by a pulsed Nd:YAG laser system. A general feature is the formation of oxygen shells. In our case they might prevent further particle regrowth on the substrate. Furthermore, it was possible to observe hydrogenation effects, both optically and electrically, even with oxide shells, giving further evidence, these shells are not noticeably impeding the hydrogenation/dehydrogenation process.

Yttrium nanoparticles seem more sensitive than yttrium films [15]. The large surface to volume ratio is probably responsible. Percolated nanoparticle films allow to put yttrium on top of the Pd catalyst, thus further increasing the reaction speed, as diffusion of hydrogen through the catalyst material is not necessary.

Optical and electrical measurements have shown the high sensitivity of this system. We can clearly see optical changes in a wide pressure range of 5×10^{-3} mbar to 8.8 mbar exploiting the disappearance of the Mie resonance structures present in metallic dihydride. Electrical measurements, taking advantage of the alteration in conductance, cover at least 6 decades, but show the largest change in pressure ranges above 10^{-2} mbar. Time resolved measurements reveal the presence of more than one diffusion regime to be present. The mechanisms are yet to be clarified.

The sensitivity of our system to low hydrogen amounts makes a future application as a hydrogen sensor feasible. Such sensors could become important for detecting hydrogen, used to replace carbon based, fossil fuel sources, for example in cars.

The authors would like to thank Dr.-Ing. H-J. Klaar from the GfE RWTH Aachen for TEM pictures presented in this paper. One of the authors (G. Bour) gratefully acknowledges the European Union, TMR Research Network Clupos. A. Stepanov is indebted to the Alexander von Humboldt Foundation for guest stipendium.

References

1. *Gmelin Handbuch der Anorganischen Chemie*, 8. Auflage, Part C1: Rare Earth Elements - Sc, Y, La und Lanthanide - Hydrides, Oxides (Springer-Verlag, Berlin, Heidelberg, New York, 1974).
2. P. van der Sluis, M. Ouwerkerk, P.A. Duine, Appl. Phys. Lett. **70**, 3356 (1997).
3. H. Flotow, D. Osborne, K. Otto, B. Abraham, J. Chem. Phys. **38**, 2620 (1963).
4. L. Yannopoulos, R. Edwards, P. Wahlbeck, J. Phys. Chem. **69**, 2510 (1965).
5. O.F. Hagena, Surf. Sci. **106**, 101 (1981).

6. O.F. Hagena, Z. Phys. D **20**, 425 (1991).
7. G. Gärtner, H. Lydtin, Nanostruct. Mat. **4**, 559, (1994).
8. R.E. Smalley, J.R. Heath, Y. Liu, S.C. O'Brien, Q.-L. Zhang, R.F. Curl, F.K. Tittel, J. Chem. Phys. **83**, 5520 (1985).
9. Q. Li, T. Sasaki, N. Koshizaki, Appl. Phys. A **69**, 115 (1999).
10. T. Sasaki, S. Terauchi, N. Koshizaki, H. Umehara, Appl. Surf. Sci. **127-129**, 398 (1998).
11. T. Makino, N. Suzuki, Y. Yamada, T. Yoshida, T. Seto, N. Aya, Appl. Phys A **35** [Suppl.] S243 (1999).
12. Z. Pástzi, Z.E. Horváth, G. Petõ, A. Karacs, L. Guczi, Appl. Surf. Sci. **109/110**, 67 (1997).
13. G. Mie, Ann. Phys. **25**, 377 (1908).
14. J. Huiberts, J. Rector, R. Wijgaarden, S. Jetten, D. de Groot, B. Dam, N. Koeman, R. Griessen, B. Hjörvarsson, Y. So, J. Alloys Comp. **239**, 158 (1996).
15. Dielectric function for $YH_{1.73}$, R. Griessen, UvA, private communication.
16. Dieletric function for $YH_{1.81}$, R. Griessen, UvA, private communication.
17. Dieletric function for $YH_{2.2}$, R. Griessen, UvA, private communication.
18. M Gartz, C. Keutgen, S. Kuenneke, U. Kreibig, Eur. Phys. J. D **9**, 127 (1999).